Planetary and Space Science 198 (2021) 105186

Contents lists available at ScienceDirect

Planetary and Space Science

journal homepage: www.elsevier.com/locate/pss

Exploiting night-time averaged spectra from PFS/MEX shortwave channel. Part 1: Temperature retrieval from the CO_2 ν_3 band

Sophie Bauduin [a,*], Marco Giuranna [b], Paulina Wolkenberg [b], Luca Nardi [c,b], Frank Daerden [d], Jimmy Bouche [a], Catherine Wespes [a], Gilles Lecomte [a], Ann Carine Vandaele [d], Pierre Coheur [a]

[a] Université libre de Bruxelles (ULB), Spectroscopy, Quantum Chemistry and Atmospheric Remote Sensing (SQUARES), Brussels, Belgium
[b] National Institute of Astrophysics INAF-IAPS, Rome, Italy
[c] University of Rome "La Sapienza", Rome, Italy
[d] Royal Belgian Institute for Space Aeronomy, Brussels, Belgium

ARTICLE INFO

Keywords:
Mars atmosphere
Temperature profile
Night measurements
Retrieval
PFS
Thermal inversion

ABSTRACT

Nadir remote sensing of the night side of Mars is challenging, mainly due to the low signal-to-noise ratio of such observations. We show in a companion paper that the abundance of carbon monoxide (CO) during night can be retrieved from the observations of the Planetary Fourier Spectrometer (PFS). This requires, however, an accurate knowledge of the temperature profile, and especially of the night-time thermal inversions, to properly model the atmospheric emission. While the temperature profile is usually retrieved from the ν_2 band of CO_2 (centered at 667 cm^{-1}), this work shows that, for averaged night-time PFS observations built from a large ensemble of spectra, the temperature profile can be retrieved from the more saturated ν_3 band of CO_2 (centered at 2349 cm^{-1}). We show especially that, due to IFOV (instantaneous field-of-view) size differences and boresight offset between the longwave and shortwave channels of PFS, the temperature profile retrieved from the ν_3 band is more consistent with the emission observed in the 1-0 band of CO (centered at 2143 cm^{-1}), which is used in the second part paper. We provide a complete characterization of the retrieved temperature profiles in terms of error and vertical sensitivity. Using this, we show that using the ν_3 CO_2 band allows to properly constrain and characterize the thermal inversions encountered near the surface for most night-time observations. The resulting set of temperature profiles is essential for the retrieval of the night-time CO abundance that is presented in the companion paper. Beyond their usefulness for the night-time CO retrieval, we suggest with a last example that temperature profiles retrieved from the ν_3 band of CO_2 could be use more generally to study surface thermal inversions encountered at night.

1. Introduction

The Martian day and night sides have not been the object of the same attention since the beginning of satellite missions around Mars. While the Martian day side has been extensively studied by remote sounders, less attention has been given to the night part. This is explained by the fact that Mars night-time remote observations are challenging to analyze, especially in nadir mode, because notably of their poor signal-to-noise ratio (SNR) associated with weak or no (at short wavelength) radiation sources. A series of works, targeting different atmospheric parameters and regions, have nevertheless successfully exploited remote observations of the night side of Mars. For instance, stellar occultations and limb soundings have been used to study different phenomena occurring in the Martian upper atmosphere, such as the nitric oxide (NO) ultraviolet night glow (e.g. Bertaux et al., 2005; Cox et al., 2008; Gagné et al., 2013; Stiepen et al., 2015, 2017) or auroras (Schneider et al., 2015). They have also been used to retrieve vertical profiles of gas density (CO_2, ozone), temperature, dust/aerosols and clouds for the night side (e.g. Quémerais et al., 2006; Lebonnois et al., 2006; Montmessin et al., 2006; Forget et al., 2009; Montmessin and Lefèvre, 2013, and references therein). Active sounding by the Mars Orbiter Laser Altimeter (MOLA) has been exploited for the detection and characterization of CO_2 clouds, particularly during the polar night (Pettengill and Ford, 2000; Ivanov and Muhleman, 2001; Colaprete and Toon, 2002; Neumann et al., 2003). The analysis of nadir night-time measurements has allowed retrieving surface temperatures and temperature profiles for the Martian night side (e.g. Smith, 2004;

* Corresponding author.
E-mail address: sbauduin@ulb.ac.be (S. Bauduin).

https://doi.org/10.1016/j.pss.2021.105186
Received 28 July 2020; Received in revised form 8 December 2020; Accepted 3 February 2021
Available online 16 February 2021

Giuranna et al., 2019b), but also the water vapour content in the low atmosphere (Pankine and Tamppari, 2015). Very recently, exploiting nadir PFS observations, Giuranna et al. (2019b) have reported the first complete daily cycle (including night) of dust and water ice optical depths, and have been also able to retrieve these parameters for the polar nights. However, the retrieval of carbon monoxide (CO) abundances from night-time nadir observations has never been reported.

The general goal of our work is to demonstrate the possibility of measuring the abundance of CO during night using the observations of the Planetary Fourier Spectrometer (PFS). The fundamental 1-0 band of CO is especially targeted. Because this band is located at the edge of the thermal infrared (TIR), a good knowledge of the temperature profile is required to properly model the atmospheric emission. In fact, during night, because the daytime convection vanishes, large thermal inversions develop close to the surface and are responsible for the occurrence of features (e.g. CO lines) in emission in PFS observations. It is crucial to properly constrain these thermal inversions to correctly model night-time PFS spectra. In most studies, temperature profiles are accurately retrieved from the ν_2 CO_2 band centered at 667 cm^{-1} (e.g. Smith, 2004; Giuranna et al., 2019b; Guerlet et al., 2018). For PFS, this relates to the longwave infrared channel (LWC). This standard way of doing has, however, turned out to be unsatisfactory for the specific goal of our work, i.e. the retrieval of the night-time CO abundance (Bauduin et al., 2020, this issue) from averaged night-time PFS observations in the shortwave channel (SWC). We show that the temperature profile can fortunately be retrieved accurately from the more saturated ν_3 band of CO_2 centered at 2349 cm^{-1} in the SWC. While these accurate temperature profiles are useful for the night-time CO retrieval performed in the companion paper, this work also shows that the ν_3 CO_2 band could be used to properly constrain and characterize the thermal inversions encountered near the surface for most night-time observations. Section 2 presents the PFS observations used in this work. Section 3 explains why an alternative for the temperature retrieval has been necessary and shows that the ν_3 CO_2 band can be exploited. Section 4 provides a characterization for the retrieved temperature profiles in terms of error and vertical sensitivity. Section 5 applies the retrieval method to a night-time spectra built from a smaller average to explore the possibility of using the ν_3 CO_2 band not only in the specific case of the night-time CO retrieval but more generally for retrieving thermal inversions. Finally, section 6 gives the conclusions.

2. Observations

In this work, we have used the observations of the Planetary Fourier Spectrometer (PFS) instrument onboard Mars Express (MEX). Details about the instrument and its calibration can be found in (Formisano et al., 2005; Giuranna et al., 2005a,b). Since January 2004, PFS has been observing the atmosphere of Mars and has collected 8 full Martian Year (27 MY to 34 MY) of Mars spectra. Among this large dataset, only night-time nadir spectra have been considered here. They have been defined as the observations for which the solar incidence angle is larger than 90°. Only PFS spectra associated to dust and ice optical depths smaller than 0.2 have been selected to simplify the radiative transfer calculations by neglecting the scattering. The dust and ice optical depths were provided as part of the PFS level 2 processed data (hereafter L2) by the National Institute of Astrophysics INAF-IAPS (Wolkenberg et al., 2018; Giuranna et al., 2019b). Since the ν_3 band of CO_2 is centered at 2349 cm^{-1}, only the observations recorded by the PFS SWC are used in this work.

Because the night-time PFS measurements have very low SNR, averaged spectra have been built from the selected set of individual observations. More specifically, the averages have been made for boxes of 10° of solar longitude (L_s) and 5° of latitude over the 8 MYs, leading to1163[1] averaged spectra in total. The choice for these averages was driven by the detection of the 1-0 CO band (centered at 2143 cm^{-1}) as explained in Bauduin et al. (2020). Among the set of averaged spectra, we use throughout this document as an example the averaged spectrum located in box 40°S-35°S/280°- 290° (Lat/L_s). The error and vertical sensitivity characterization are performed on a subset of 170 averaged night-time observations, which is shown in Fig. 1. These averaged spectra correspond to those for which CO has been detected and successfully retrieved (Bauduin et al., 2020).

[1] Some boxes do not include averaged spectra, due to some of the selection criteria.

3. Choice of the CO_2 band for the temperature retrieval

As introduced, the temperature profile retrievals usually rely on the information contained in the ν_2 band of CO_2 centered at 667 cm^{-1}. This section demonstrates that for the particular case of averaged night-time PFS SWC observations, the use of the CO_2 ν_3 band provides better results and in particular that its use is crucial to properly model the thermal inversions generally encountered at night.

3.1. Background

As already mentioned, a good knowledge of the temperature profile of the Martian atmosphere is essential to properly model TIR spectra and thus to retrieve relevant CO abundances. For the analysis of each night-time average spectrum, we have initially built an associated temperature profile by calculating the mean of all temperature profiles associated to the single spectra used for the spectral average (Fig. 2c). These single observations temperature profiles, provided as part of the PFS L2 by the National Institute of Astrophysics INAF-IAPS (Wolkenberg et al., 2018; Giuranna et al., 2019b), are retrieved from the CO_2 ν_2 band. Fig. 2 shows in blue examples of calculated spectra using this average temperature profile in the region of the ν_2 (Fig. 2a) and ν_3 (Fig. 2b) CO_2 bands (details about the simulation settings are given in section 3.2.2). The surface temperature of 218 K corresponds to the average of the surface temperature from the L2. The ν_2 band is well modelled, which means that, according to this band, the averages calculated from the L2 are good estimations of the surface temperature and temperature profile. However, it is clear that the ν_3 band is not well reproduced. A surface temperature of 218 K is definitely too low to properly model the baseline of the spectrum. It is more reasonably around 224 K as observed in Fig. 2 b with the red curve (note that this leads to an overestimation of the baseline for the ν_2 band, Fig. 2a). Even using 224 K for the surface

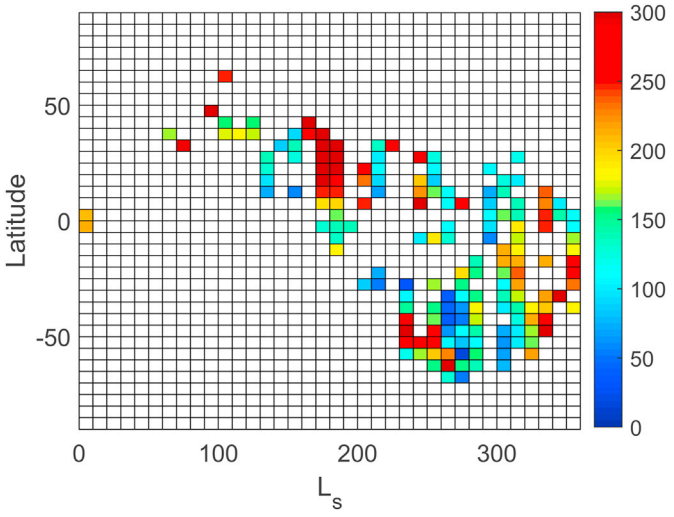

Fig. 1. Selected averaged night-time PFS spectra for this work. This selection is based on the detection of CO and on the success of the CO retrieval (Bauduin et al., 2020). The color scale indicates the number of PFS night-time observations averaged together.

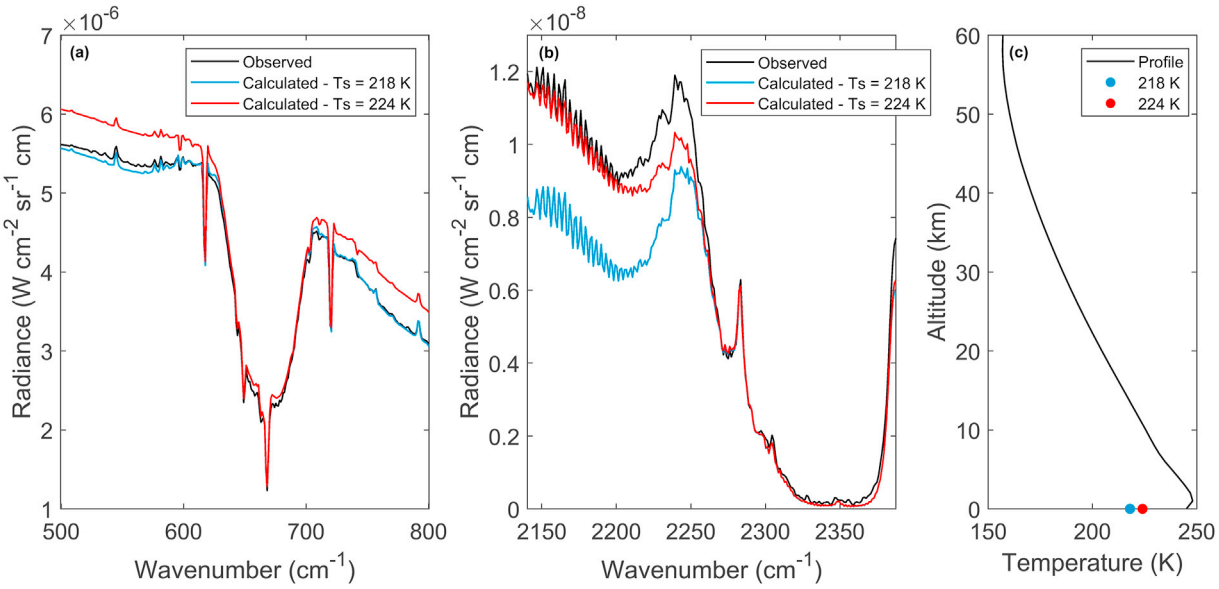

Fig. 2. Observed and calculated PFS spectra in the range of the ν_2 (a) and of the ν_3 (b) CO_2 bands. The calculated spectra have been computed using the average temperature profile built from the L2 temperature profiles and shown in panel (c). Two different surface temperatures have been considered: 218 K (blue) and 224 K (red). The simulations have been done with the settings given in section 3.2.2. The emissivity has been fixed to 0.97 for the range of the ν_2 band (Bandfield, 2002) and to 0.9 for the ν_3 band.

temperature, there is still a clear lack of emission in the wings of the ν_3 CO_2 band. Since the surface temperature is pretty well constrained, this lack of emission can only be compensated by adjusting the temperature profile, and especially the thermal inversion, which should be shifted towards higher temperatures.

The above discussion suggests that the two CO_2 bands are not consistent with each other. This is not surprising considering the two following observational characteristics of PFS:

1. The offset between the boresights of the two channels. It is around 1°, which means that on the Martian ground, the distance between the boresights depends on the PFS altitude. The higher the MEX spacecraft altitude, the larger the spatial separation of the two PFS footprints. Fig. 3 shows the distribution of the distance between the SWC and LWC boresights among the single spectra used to built the average shown in Fig. 2. For this particular example, 63% of the spectra present a distance between the SWC and LWC boresights smaller than 20 km; these spectra are taken close to the pericentre altitude (around 240 km). The rest of the spectra present larger differences, up to 180 km. In these cases, the spectra taken by the LWC and the SWC probe different regions and air masses. The inclusion of such spectra in the average can therefore lead to some inconsistencies between the two channels.
2. The size difference between the instantaneous field-of-view (IFOV) of the SWC and the LWC channels of PFS, which are respectively of 1.52° (full width at half maximum, FWHM) and of 2.69°. At the pericentre altitude, and close to nadir, the size difference between the two channels is relatively small (the spatial resolution is indeed respectively of 6.5 km and 11.5 km for the SWC and LWC), but at higher altitude, this difference is much larger. As an example, when PFS is at 8000 km, the spatial resolution is around 220 km and 390 km respectively for the SWC and the LWC. As a result, the LWC observes a much larger area than the SWC. The effect increases with increasing zenith angle. In building the average spectra for the CO retrieval, no selection has been made on either the PFS altitude or the zenith angle. In the spectral averages, PFS spectra taken at high altitude/high zenith angle are thus included. For instance, around 37% of the spectra included in the average of the example shown in Fig. 2 are taken at altitudes higher than 3000 km. Due to the different IFOV size between the SWC and LWC channels, the final averaged spectra for both channels are not completely equivalent.

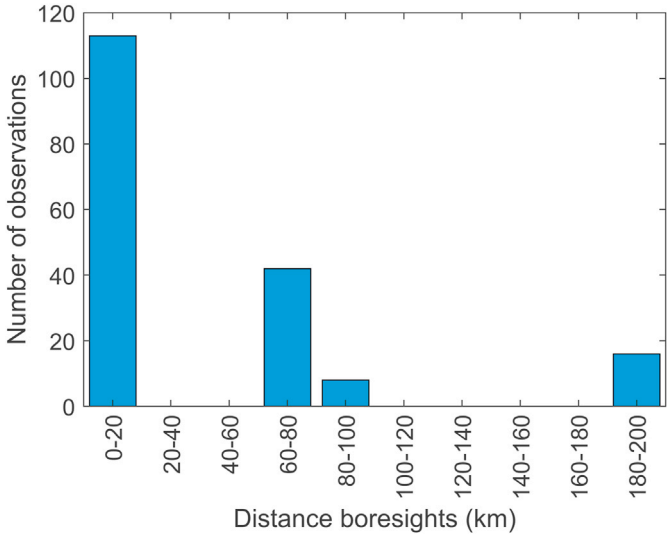

Fig. 3. Histogram of the distance between the SWC and LWC boresights among the spectra used in the spectral average of the example shown in Fig. 2.

It is worth noting that this inconsistency between the two CO_2 bands has not been observed in the analysis of daytime single spectra (Bouche et al., 2019) recorded at emission angle close to nadir and when PFS is close to the pericentre altitude. In these conditions, the IFOV differences between the LWC and the SWC mentioned above are minimized. This is also the case when averaged daytime spectra are built from several single observations recorded at small emission angles and close to the pericentre altitude (Giuranna et al., 2019b). In these cases, the temperature profile retrieved from the LWC observations can satisfactorily be used for retrievals exploiting both the SWC and LWC. For the purpose of this work, temperature profiles retrieved from the less frequently used ν_3 band proves to be a better choice. Indeed, as the 1-0 band of CO, the CO_2 ν_3 band is located in the spectral range covered by the SWC of PFS. The

surface temperature and temperature profile retrieved from this band are therefore more consistent with the SWC observation, and thus with the 1-0 band of CO. Even if the ν_3 is partly saturated, it contains information about atmospheric temperatures, especially in its wings. This is well observed in Fig. 4, showing the temperature Jacobians[2] for the ν_3 band spectral range and for altitudes from 0 to 60 km. It can be seen that the sensitivity to temperature from this band goes from 0 to around 30 km, with maximal sensitivity originating from the wings (around 2250 cm^{-1}) and for the altitude range 0–10 km, where the thermal inversion is located (Fig. 2). In the following sections, we compare the temperature retrievals using both CO_2 bands and then we show that only the one retrieved from the ν_3 band provides a satisfactory input for the CO retrieval.

3.2. Test of temperature retrieval using two different CO_2 bands

3.2.1. Retrieval methodology

In this work, the Optimal Estimation (OE) (Rodgers, 2000) is used to retrieve the temperature profile. The idea of the method is to find the temperature profile that is the most consistent with both the averaged night-time spectrum and the prior knowledge of the Martian atmosphere. This is done by minimizing a cost function J, written as:

$$J = (\mathbf{y} - \mathrm{F}(\mathbf{x}, \mathbf{b}))^{\mathrm{T}} \mathbf{S}_{\boldsymbol{\varepsilon}}^{-1} (\mathbf{y} - \mathrm{F}(\mathbf{x}, \mathbf{b})) + (\mathbf{x} - \mathbf{x}_{\mathrm{a}})^{\mathrm{T}} \mathbf{S}_{\mathbf{a}}^{-1} (\mathbf{x} - \mathbf{x}_{\mathrm{a}}), \quad (1)$$

where $\mathbf{x}$ is the atmospheric state vector, including the parameters to retrieve, $\mathbf{b}$ includes the parameters affecting the TOA radiance but that are kept fixed, $\mathbf{y}$ is the vector of measured radiances, $\mathbf{x_a}$ is the *a priori* state vector, including the knowledge of the retrieved parameters before the measurement is made, $\mathbf{S_a}$ is the associated *a priori* covariance matrix, $\mathbf{S_\varepsilon}$ is the measurement error covariance matrix associated to $\mathbf{y}$ and F is the radiative transfer forward model. The minimization of J is performed by a Gauss-Newton iterative scheme (Rodgers, 2000), with a new state vector evaluated at each iteration i as follow:

$$\mathbf{x}_{i+1} = \mathbf{x}_{\mathrm{a}} + \left(\mathbf{K}_i^{\mathrm{T}} \mathbf{S}_{\boldsymbol{\varepsilon}}^{-1} \mathbf{K}_i + \mathbf{S}_{\mathrm{a}}^{-1}\right)^{-1} \mathbf{K}_i^{\mathrm{T}} \mathbf{S}_{\boldsymbol{\varepsilon}}^{-1} [\mathbf{y} - \mathrm{F}(\mathbf{x}_i, \mathbf{b}) + \mathbf{K}_i (\mathbf{x}_i - \mathbf{x}_{\mathrm{a}})], \quad (2)$$

with $\mathbf{K}$ the Jacobians matrix, whose rows are the derivatives of the TOA radiance with respect to the retrieved parameters. For more details about the method, see (Rodgers, 2000).

3.2.2. Temperature retrieval from ν_2 and ν_3 CO_2 bands

The temperature retrieval has been tested on the example case of Fig. 2. It has been performed on the 500–800 cm^{-1} and on the 2140–2387 cm^{-1} spectral ranges respectively for the ν_2 and ν_3 CO_2 bands. The *a priori* profile has been taken in both cases as the average temperature profile calculated from the L2. The *a priori* variability (square root of the diagonal elements of $\mathbf{S_a}$) has been set to 2 K. This value allows sufficient variability for the retrieval while providing sufficient constraint to avoid retrieved temperature profiles that present unrealistic large vertical oscillations. To take into account the correlation between the atmospheric levels, the off-diagonal elements have been calculated using an exponential decay from the diagonal (Rodgers, 2000) and considering a correlation length of one scale height. Assuming an average temperature of 210 K and a molar mass of 43 g/mol, the scale height of Mars' atmosphere is 11 km. The temperature has been retrieved on the altitude range from 0 km to 60 km by steps of 1 km between 0 and 10 km, and by steps of 2 km from 10 to 60 km. As temperature and CO_2 abundance are correlated in the radiative transfer, the CO_2 profile cannot be retrieved simultaneously to the temperature and must be kept fixed. However, its choice, and thus that of the pressure profile, is critical. While there is clearly no perfect option for averaged spectra, the way we have proceeded is the following. We have calculated the average surface pressure from the Mars Climate Database version 5.3 for each average PFS spectrum. Using this average surface pressure and the hydrostatic equation, the rest of the pressure profile has been calculated for the *a priori* temperature profile. The CO_2 VMR profile was set to a global average calculated from the Mars Climate Database (MCD, version 5.3) (Forget et al., 1999; Millour et al., 2018) (see Bouche et al. (2019) for details). Such assumptions lead to uncertainties on the retrieved temperature profile, which we will discuss in section 4. The surface temperature has been retrieved simultaneously with the temperature profile to properly model the spectrum baseline. The *a priori* value has been set to 218 K (the average surface temperature calculated from the L2) and an *a priori* variability of 2 K has been considered. For the ν_2 spectral range, the emissivity has been fixed to 0.97 according to Bandfield (2002). For the ν_3 spectral range, it has been fixed to 0.9; it corresponds to the emissivity average value calculated by co-localizing single spectra with the emissivity at 2000 cm^{-1} global maps provided by the Planetary SUrface Portal (Poulet et al., 2018; Quantin-Nataf et al., 2018). Finally, the spectroscopic parameters have been taken from HITRAN 2016 (Gordon et al., 2017), including the pressure broadening by CO_2, and the instrumental line shape recommended by the PI team of PFS has been considered (Giuranna et al., 2019a).

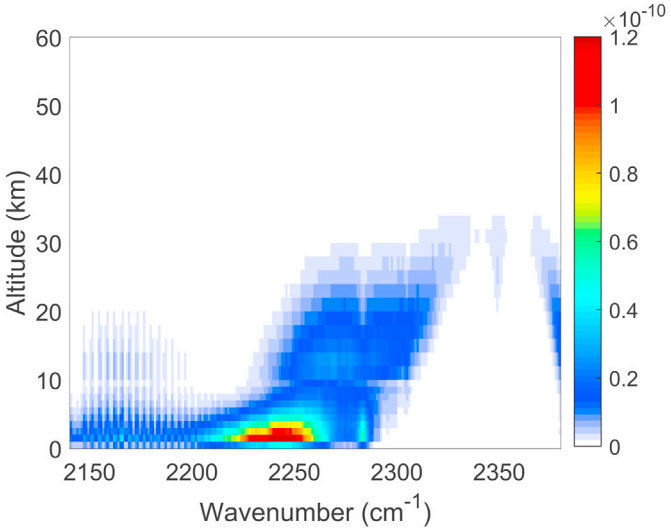

Fig. 4. Temperature Jacobians (W/(cm^2 sr cm^{-1} K), color scale) calculated for the ν_3 spectral range and for altitudes from 0 to 60 km.

Fig. 5 shows the results of the temperature retrieval performed on the two CO_2 bands. The two retrievals are successful and the fits are of very good quality. The root mean squares of the residuals is similar to the noise level considered (RMS = 2.90×10^{-8} W/(cm^2 sr cm^{-1}) for a noise = 2.25×10^{-8} W/(cm^2 sr cm^{-1}) for the ν_2 band; RMS = 1.47×10^{-10} W/(cm^2 sr cm^{-1}) for a noise = 1.87×10^{-10} W/(cm^2 sr cm^{-1}) for the ν_3 band). As expected, however, the two retrieved temperature profiles shown on panel (c) are significantly different. The temperature profile retrieved from the ν_2 band is logically very close from the *a priori* (average temperature profile) and the retrieved surface temperature is 219 K. For the ν_3 band, the retrieved temperature profile is hotter than the *a priori*, to reproduce the emission in the wing of the ν_3 band. The retrieved surface temperature is 224 K. The retrieval errors are similar for the two bands (see also section 4).

3.2.3. Test of the retrieved temperature profiles for the CO retrieval

Using the two temperature profiles retrieved in previous section, we have retrieved the CO profile. The procedure follows the one described by Bouche et al. (2019) and is fully presented in the companion paper (Bauduin et al., 2020); note at this point that in addition to CO, the surface temperature is again retrieved. Fig. 6 shows the results for both

[2] Derivatives of the top of the atmosphere (hereafter TOA) radiance with respect to the temperature at different altitude levels.

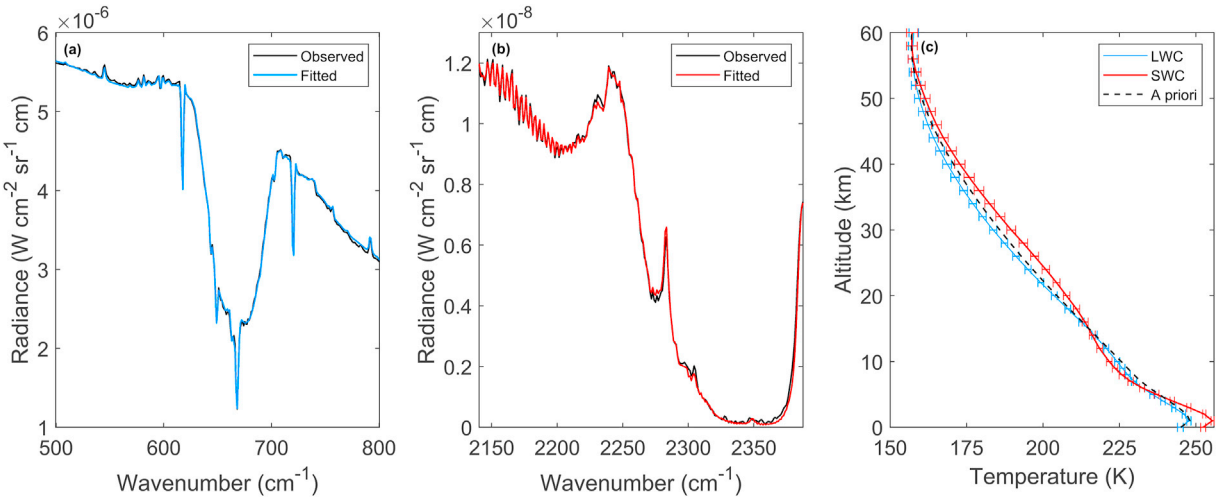

Fig. 5. Temperature retrieval for one example of average PFS observation using the ν_2 (a) and ν_3 (b) bands of CO_2. Panel (c) shows the retrieved temperature profiles (blue for ν_2 and red for ν_3) with the associated retrieval errors. The latter correspond to the square root of the diagonal elements of the error covariance matrix.

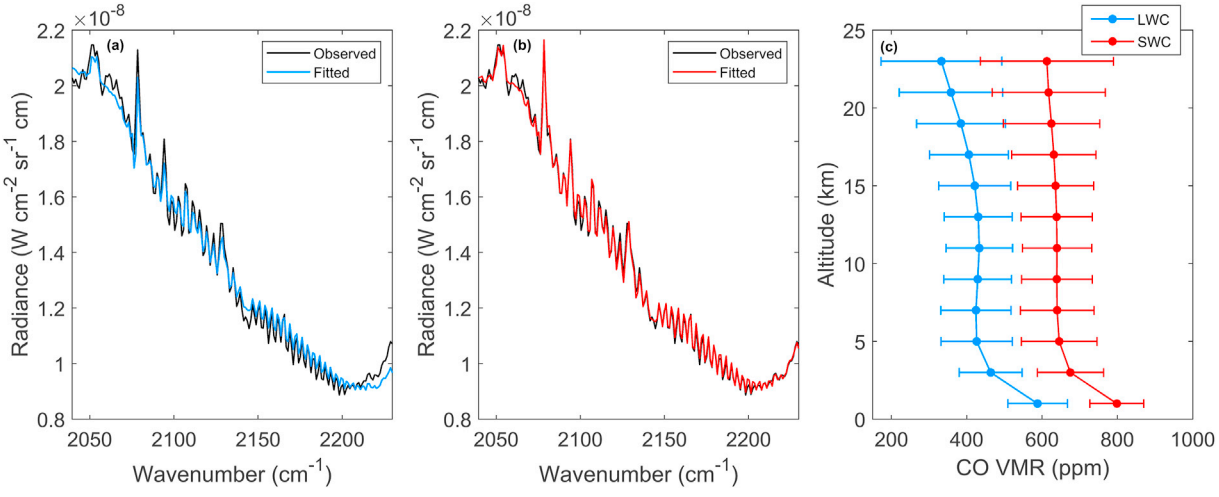

Fig. 6. Retrieval of the CO vertical profile using the temperature profiles retrieved from the ν_2 CO_2 band (a) and from the ν_3 CO_2 band (b). Panel (c) shows the retrieved CO profiles.

retrievals. The first thing to note is that the choice of the temperature profile significantly influences the retrieved CO abundance (as seen in Fig. 6c). The difference can be up to 200 ppm. Then, we clearly see that the best fit is obtained when using the temperature profile retrieved from the ν_3 band. Indeed, there is a clear misfit in the R-branch of the 1-0 CO band when using the temperature profile retrieved from the ν_2 band (Fig. 6a). Moreover above 2200 cm^{-1}, where the ν_3 CO_2 band starts, the shape of the emission in the band wing is not well modelled. Finally, when compared to Fig. 6 b, there is a lack of emission in the CO_2 Q-branches located at 2078.4 cm^{-1} and 2094.2 cm^{-1}. These misfits are due to the temperature inconsistencies between the two bands. When the temperatures retrieved from the ν_2 band are used as input for the CO retrieval, the retrieved surface temperature reaches 225 K to model the baseline in the 1-0 band. As a consequence, because the temperature profile is kept fixed during the CO retrieval, the amount of emission in the near-surface atmosphere is reduced and leads to some of the mentioned effects in Fig. 6 a.

According to the above discussion, we conclude that, for the retrieval of CO from averaged SWC night-time spectra, the ν_3 band of CO_2 must preferably be used. It provides a representation of the thermal inversion the most consistent with the SWC spectral range, which in turn is crucial to correctly model the emission in the 1-0 band of CO.

3.3. *Effect of the emissivity*

As seen in previous sections, one of the inconsistencies observed between the ν_2 and ν_3 CO_2 bands is the surface temperature. Indeed, one value cannot properly model the baseline for both bands. One other parameter affecting the baseline that we have not mentioned yet is the emissivity. It has been considered fixed for the two spectral ranges and equal to 0.97 and 0.9 respectively for the ν_2 and ν_3 bands. Any uncertainty on these values would lead to the estimation of different surface temperatures and could therefore be responsible for part of the observed inconsistency. Fig. 7 shows the effect of emissivity in both spectral ranges. In the region of the ν_2, the simulations are performed for two emissivity values and considering the surface temperature retrieved from the ν_3 band (224 K). Conversely for the latter, the same two emissivity values are tested along with the surface temperature retrieved from the ν_2 band (218 K). From Fig. 7 a, we can see that for the ν_2 band spectral range, if the emissivity is taken equal to 0.9 instead of 0.97, a surface temperature of 224 K becomes more consistent with this spectral range. However, increasing the emissivity from 0.9 to 0.97 for the ν_3 band spectral range has less impact; even with a higher emissivity, a surface temperature of 218 K remains too low to properly model the baseline for this spectral range (Fig. 7b).

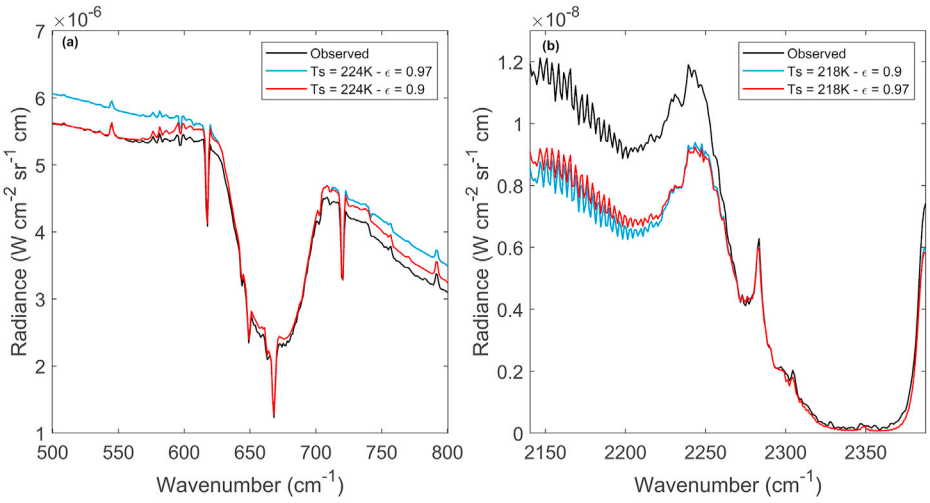

Fig. 7. Observed and calculated spectra in the range of the ν_2 (a) and ν_3 (b) CO_2 bands. The spectra are calculated for both bands using two different values for the emissivity: 0.97 and 0.9. The surface temperature is taken equal to 224 K and 218 K respectively for the ν_2 and the ν_3 bands.

Still, assuming that an error on the emissivity could be responsible for the temperature inconsistencies described previously, we have investigated if considering an emissivity of 0.9 for the ν_2 CO_2 band would allow retrieving a temperature profile similar to the one from the ν_3 spectral range. The goal is also to verify if such error could change the choice of the CO_2 band for the temperature retrieval. For this, we have followed the method described in section 3.2: we have first retrieved the temperature profile from the ν_2 band considering an emissivity of 0.9, and we have then retrieved the CO profile. The retrieval settings are those described in section 3.2.2. The results are shown in Fig. 8. The first thing

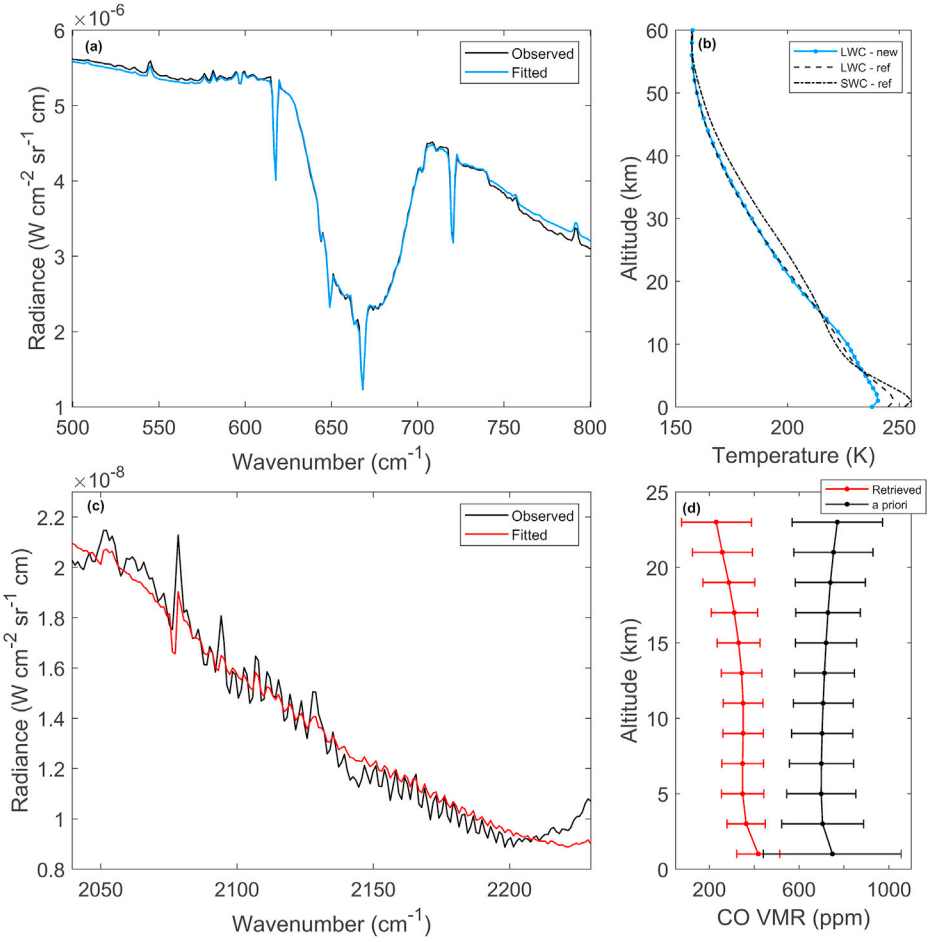

Fig. 8. (a,b) Retrieval of the temperature profile from the ν_2 CO_2 band using an emissivity of 0.9. The dashed line in panel b corresponds to the temperature profile retrieved from the same spectral range but using an emissivity of 0.97 (see Fig. 5a) and the dashed-dotted line correspond to the temperature profile retrieved from the ν_3 band (see Fig. 5b). These two profiles are taken as our references. (c,d) Retrieval of the CO profile using the temperature profile retrieved in panel b (blue).

to notice is that the fit of the ν_2 band is reasonable (RMS equal to 5.10×10^{-8} W/(cm^2 sr cm^{-1})), except for the edges of the spectral range considered. It is, however, not as good as that obtained using an emissivity of 0.97 (Fig. 5 a; RMS of 2.90×10^{-8} W/(cm^2 sr cm^{-1})). Fig. 8 b shows the retrieved temperature profile (blue) along with the profiles retrieved previously (section 3.2.2) from the ν_2 band using an emissivity of 0.97 (dashed line) and from the ν_3 band with an emissivity of 0.9 (dashed-dotted line). The last two are taken as our references. We can see that the retrieved profile is colder than the two reference temperature profiles close to the surface (below 5 km) and then stays close to the reference profile retrieved from the ν_2 CO_2 band. The retrieved surface temperature is 223.5 K. This means that, considering these temperatures, the intensity of the emission close to the surface is smaller than for the two reference cases. This is well observed in Fig. 8 c, which shows the fit for the CO retrieval performed with the new temperatures. The fit of the 1-0 band of CO is very poor in three different ways. Firstly, the intensity of the CO lines is not properly modelled. This is partly related to the shape of the baseline that is badly reproduced, more particularly in the R-branch of the 1-0 band of CO. Secondly, the temperature profile considered does not allow to properly model the emission in the wing of the ν_3 CO_2 band (above 2200 cm^{-1}). Finally, there is a clear lack of emission in the CO_2 Q-branches located at 2078.4 cm^{-1} and 2094.2 cm^{-1} (note that the Q-branch at 2078.4 cm^{-1} is even partly in absorption). In conclusion, while using a smaller emissivity for the 500–800 cm^{-1} range reconciles the surface temperatures retrieved in the LWC and SWC, it increases the difference between the retrieved temperature profiles. As a result, the fit quality of the CO 1-0 band is even worse than in the case shown in Fig. 6 a.

4. Characterization of the retrieved temperature profiles

We characterize in this section the temperature profiles retrieved from the CO_2 ν_3 band in terms of error and vertical sensitivity. This is performed on the selected set of averaged spectra described in section 2.

4.1. Error budget

To estimate the uncertainty on the retrieved temperature profiles, we have first considered the total error covariance matrix $\mathbf{S_{tot}}$ that can be written as:

$$\mathbf{S}_{\mathrm{tot}} = \mathbf{S}_{\mathrm{s}} + \mathbf{S}_{\mathrm{m}} + \mathbf{S}_{\mathrm{f}}, \quad (3)$$

where $\mathbf{S_s}$ is the covariance matrix of the smoothing error, resulting from the limited vertical resolution of PFS, $\mathbf{S_m}$ is the covariance matrix of the measurement error, and $\mathbf{S_f}$ is the covariance matrix of the fitted parameters error, taking into account the interferences between the retrieved temperature profile and the rest of the state vector (surface temperature). The square root of its diagonal elements provide therefore the total error for the retrieved temperature at each level and includes the contribution of the smoothing error, the measurement error and of the fitted parameters. Note that the contribution of the latter is negligible compared to the two other sources. It is also important to keep in mind that these retrieval errors are partly impacted by the choice of the *a priori* variability, which by definition fixes the maximal value for the retrieval errors. The distribution of the total error for the analysed set is shown in Fig. 9 a for several retrieved altitudes. We can see that below the altitude of 10 km, it is smaller than 1.0 K for the majority of the retrievals. The total retrieval error then increases with height to reach around 2 K above 50 km. Using the error profiles of each temperature retrieval, we have calculated the mean error vertical profile. It is shown in Fig. 9 b. The smallest average error is found at 2 km and is 0.7 K. The mean error profile of Fig. 9 b will be used to estimate the propagation of the temperature retrieval error on the CO abundance retrieval in the companion paper (Bauduin et al., 2020).

The error coming from the uncertainty on the CO_2 density, and thus, on the pressure profile, is not considered in the budget of Fig. 9. As mentioned in section 3.2.2, the CO_2 abundance cannot be retrieved simultaneously with the temperature profile as these two parameters are correlated. Any uncertainty on the CO_2 abundance (and so on the pressure profile) obviously propagates to the temperature profile. The choice of the pressure profile to use for the retrieval is in our case particularly complicated, as a large number of PFS spectra, which are taken at different locations and so at different surface pressures, are averaged together. As explained in section 3.2.2, the procedure we have chosen is to calculate the mean surface pressure (from the MCD version 5.3) for each averaged spectrum and, using the equation of hydrostatic equilibrium, to estimate the pressure profile. For each averaged spectrum, we have also calculated the standard deviation of the surface pressure; its mean value, 0.9 hPa, has been considered as the uncertainty on the surface pressure. To evaluate how this uncertainty propagates on the temperature retrieval, we have retrieved new temperature profiles for all the analysed set but applying ±0.9 hPa on the surface pressure (note that the pressure profile is also modified through the hydrostatic equation).

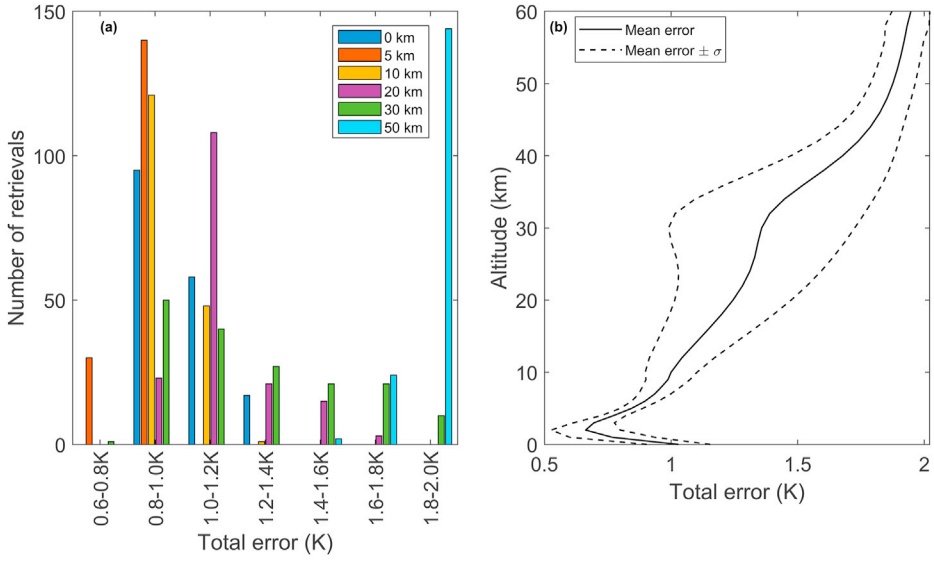

Fig. 9. (a) Histogram of the number of retrievals as a function of the total retrieval error for different altitudes. (b) Mean error profile (K) and its associated standard deviation.

The mean differences between the new and the reference temperature profiles are taken as the uncertainty on the temperature profile due to the uncertainty on the pressure (the temperature-pressure error). They are shown in Fig. 10. They are very similar and (almost) symmetric. The largest uncertainty is found around 10 km and reaches −3.5 K and 4.5 K respectively for a surface pressure shift of +0.9 hPa and −0.9 hPa. These uncertainties on the temperature profile will in turn be propagated on the retrieval of CO (Bauduin et al., 2020). Note finally that even if only spectra associated with a dust optical depth lower than 0.2 have been selected, because we have neglected the scattering some additional errors might contribute to the total error on the temperature profile. However, these errors should be low given the fact that scattering by dust does not contribute significantly to the spectral range considered (Billebaud et al., 2009).

4.2. Vertical sensitivity

The vertical sensitivity of the temperature retrieval is evaluated here with the averaging kernel functions (AVK), defined as the rows in the averaging kernel matrix **A**:

$$\mathbf{A} = \left(\mathbf{K}^{\mathrm{T}}\mathbf{S}_{\varepsilon}^{-1}\mathbf{K} + \mathbf{S}_{\mathbf{a}}^{-1}\right)^{-1}\mathbf{K}^{\mathrm{T}}\mathbf{S}_{\varepsilon}^{-1}\mathbf{K}. \quad (4)$$

One AVK is associated to the temperature retrieved at each level. It peaks at the altitude from where most of the information about the temperature at that level is coming. The AVK functions provide therefore an estimation of the height of maximum sensitivity to temperature of the retrieval. The trace of **A** corresponds to the degrees of freedom for signal (DOFS), which is the number of components/patterns in the retrieved profile that are measured independently of the *a priori* profile.

Fig. 11 a shows the AVK functions for the example retrieval (Fig. 5b). For display purposes and because the sensitivity of PFS is limited in the high atmosphere, they are shown for the first 50 km. We can see that the retrieval is sensitive to temperature over a broad altitude range, with several AVK functions peaking in the region 0–30 km. Above 30 km, the AVK drop close to 0 showing that the retrieval becomes insensitive to temperature. One important result is that the maximum sensitivity is found at 1 km, where the 1 km AVK peaks at a maximal value of 0.4. This is in fact the height where the thermal gradient passes from positive to negative (Fig. 5c). The thermal inversion is therefore well constrained by the retrieval from the ν_3 CO_2 band. This is also observed for the rest of the analysed set. Fig. 11 b shows the distribution of the altitude associated to the maximal value of the AVKs. It can be seen that 96% of the retrievals present a maximal AVK value between 0 and 4 km. This altitude range corresponds also to the thermal inversion, and more specifically where the temperature gradient change, for 96% of the analysed set (Fig. 11c). Regarding the range of sensitivity to temperature, it varies from 0-20 km to 0–45 km in the best cases. Finally, the DOFS varies between 3 and 5 for a large majority (90%) of the retrievals (Fig. 11d), showing that 3 to 5 patterns in the retrieved profiles are retrieved independently of the *a priori* profile.

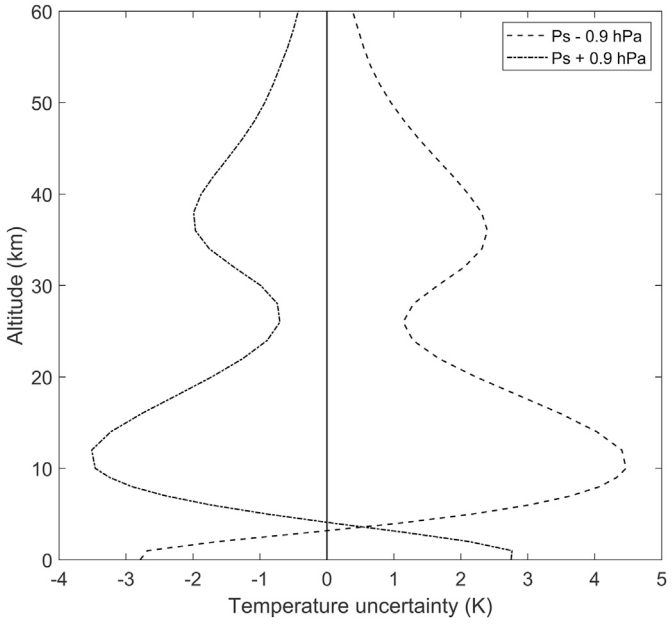

Fig. 10. Uncertainty on the temperature profile due to uncertainty on the surface pressure and profile. One curve gives the uncertainty for a shift of −0.9 hPa for the surface pressure (dashed line) and the other gives the uncertainty for a shift equal to +0.9 hPa (dashed-dotted line).

5. Beyond the night-time CO retrieval

In the previous sections, we have shown that for the analysis of SWC averaged spectra, built from a large ensemble of single observations, the temperature profile should be retrieved from the ν_3 band of CO_2 to avoid inconsistencies between the SWC and LWC due to their IFOV sizes differences and offsets. A full characterization has been performed and shows that the ν_3 band of CO_2 allows to properly retrieve the thermal inversions occurring near the surface. However, the temperature retrievals have been performed until now in the specific context of the night-time CO retrieval, and so have been performed on average spectra, built from a large set of single observations spanning different Martian Years, local times, etc. The retrieved temperatures correspond in these cases more to effective temperatures and are difficult to interpret geophysically. This section explores the possibility to exploit the ν_3 band of CO_2 on average spectra, built from a smaller and more consistent ensemble of PFS spectra, to retrieve night-time temperature profiles, and more specifically the near-surface thermal inversions, that are more geophysically interpretable.

For this, we have built a new average spectrum from a smaller ensemble of PFS SWC observations. More particularly, only 7 single SWC spectra have been used, allowing sufficient SNR in the wings of the ν_3 band of CO_2. All were recorded in MY 29 at around 23:06 local time and at $L_s = 243.52°$ in a small area spanning −60.95° to −60.72° in longitude and −43.52° to −35.93° in latitude. It is shown in Fig. 12 a. It has been analysed using the same retrieval methodology described in sections 3.2.1 and 3.2.2. The resulting fit is shown in Fig. 12a and is of good quality (RMS = 4.65×10^{-10} W/(cm^2 sr cm^{-1})) for a noise of 9.45×10^{-10} W/(cm^2 sr cm^{-1})). The retrieved temperature profile and the associated errors (only the temperature retrieval error) are shown in Fig. 12 b. The retrieved profile differs from the *a priori* profile by several K and, as already explained previously, is shifted towards higher temperature to properly reproduce the emission in the wings of the CO_2 ν_3 band. The retrieval temperature errors are within 1 K and 2 K for the entire profile as also observed for the retrieval performed on broad averages. Note that there is still an uncertainty due to the choice of the surface pressure and profile. However, since the averaged spectrum is built from a smaller ensemble of spectra, closely recorded in time and space, this uncertainty is lower than what has been estimated in section 4.1. In the specific case discussed here, the standard deviation on the surface pressure is 0.2 hPa leading to a temperature pressure error within 0.1 K and 0.5 K (in absolute value). Fig. 12c and 12 d show respectively the averaging kernel functions and the Jacobians of temperature. As observed with both panels, the sensitivity of the retrieval to temperature extends from 0 km to 40 km. The maximum sensitivity to temperature is found in the wings of the ν_3 band of CO_2 and is located close to the surface, between 1 and 2 km of height, where the AVK functions associated to the first levels peak. This is also the height where the thermal gradient passes from positive to negative (Fig. 12b).

The results discussed in this section suggest that the methodology developed for the temperature retrieval in the specific context of measuring night-time CO abundances can be applied more generally for

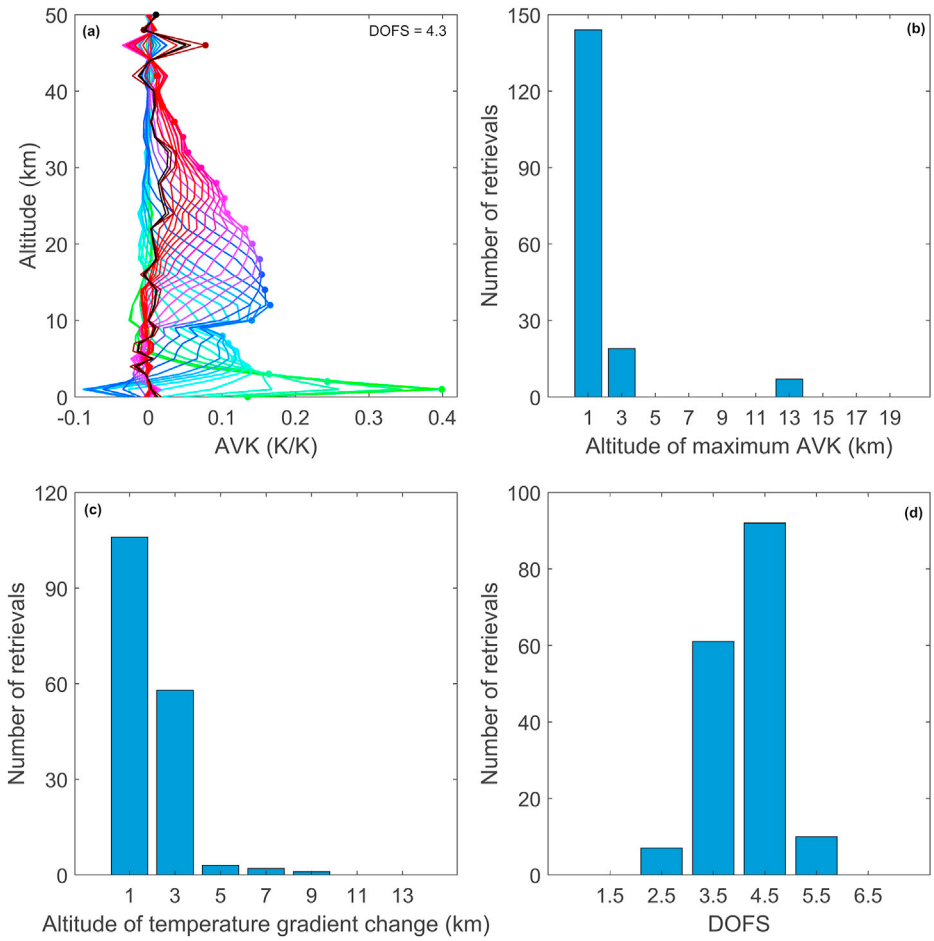

Fig. 11. (a) AVK functions from 0 to 50 km for the example retrieval of Fig. 5 b. The dots indicate to which level the AVK correspond. (b) Histogram of the number of retrievals as a function of the altitude where the largest AVK value is found. (c) Histogram of the number of retrievals as a function of the altitude where temperature gradient becomes negative. (d) Histogram of the number of retrievals as a function of the DOFS. For the three histograms, the centres of the intervals are indicated.

the retrieval of night-time temperature profiles and especially for the characterization of night-time thermal inversions. The temperature profiles retrieved from the ν_3 band of CO_2 could therefore complement the temperature profiles usually retrieved from the ν_2 band at 667 cm^{-1}.

6. Conclusion

This work has demonstrated the possibility of retrieving the temperature profile from the ν_3 band of CO_2 (centered at 2349 cm^{-1}) in the SWC of PFS. This has been particularly shown for averaged night-time PFS observations, in the more general context of measuring the night-time CO abundance. In this specific context, it has been necessary to average large ensembles of PFS night-time spectra to increase their SNR and to allow the detection of CO. Because of this, we have shown that exploiting the ν_2 band of CO_2 in the LWC, as traditionally done for the temperature retrieval, turned out to provide unsatisfactory fits for CO. This is likely related to differences between the SWC and LWC IFOV sizes and the offset between the boresights of the two channels, which make the surface temperatures and temperature profiles retrieved from the ν_2 spectral range (LWC) inconsistent with the SWC averaged spectra. In particular, the use of the temperature profile retrieved from the CO_2 ν_2 band (LWC) did not allow to properly model the atmospheric emission observed in the SWC spectral range. We have shown that the information contained in the wings of the more saturated ν_3 CO_2 band could be successfully used for the temperature retrieval of averaged night-time spectra in the SWC, in particular if associated to a large temperature inversion in the low atmosphere. It is worth mentioning that this alternative is not necessarily needed for the analysis of daytime single PFS spectra recorded at small emission angles (close to nadir) and close to the pericentre altitude of PFS (240 km). In these cases, the spatial effects due to the IFOV differences between the LWC and SWC are minimized and the temperature profile retrieved from the LWC observations can satisfactorily be used for retrievals exploiting either SWC or LWC observations. This is also the case when analysing averaged daytime spectra built from several single observations recorded at small emission angles and close to the pericentre altitude.

The temperature retrieval has been performed with the Optimal Estimation method. We have also used the framework of this method to perform a complete characterization of the temperature profiles retrieved from 170 averaged night-time PFS spectra. We have shown that the thermal inversion is well constrained for most of the retrievals; the maximal sensitivity to temperature is indeed found between 0 and 4 km where the thermal gradient changes sign. More generally, the retrieval is sensitive to temperature in the altitude range 0–20 km in the worst cases and to 0–45 km in the best cases. A complete error budget has been realized on the temperature profiles. Two types of temperature error have been distinguished and evaluated separately. The temperature retrieval errors, including the smoothing and measurement errors, have been estimated to be within 0.7 K and 2 K depending on the altitude. In addition to this error, the uncertainty on the pressure (CO_2) profile has been propagated to the temperature profile retrieval. This temperature-pressure error is found to be the largest at 10 km and about −3.5 K

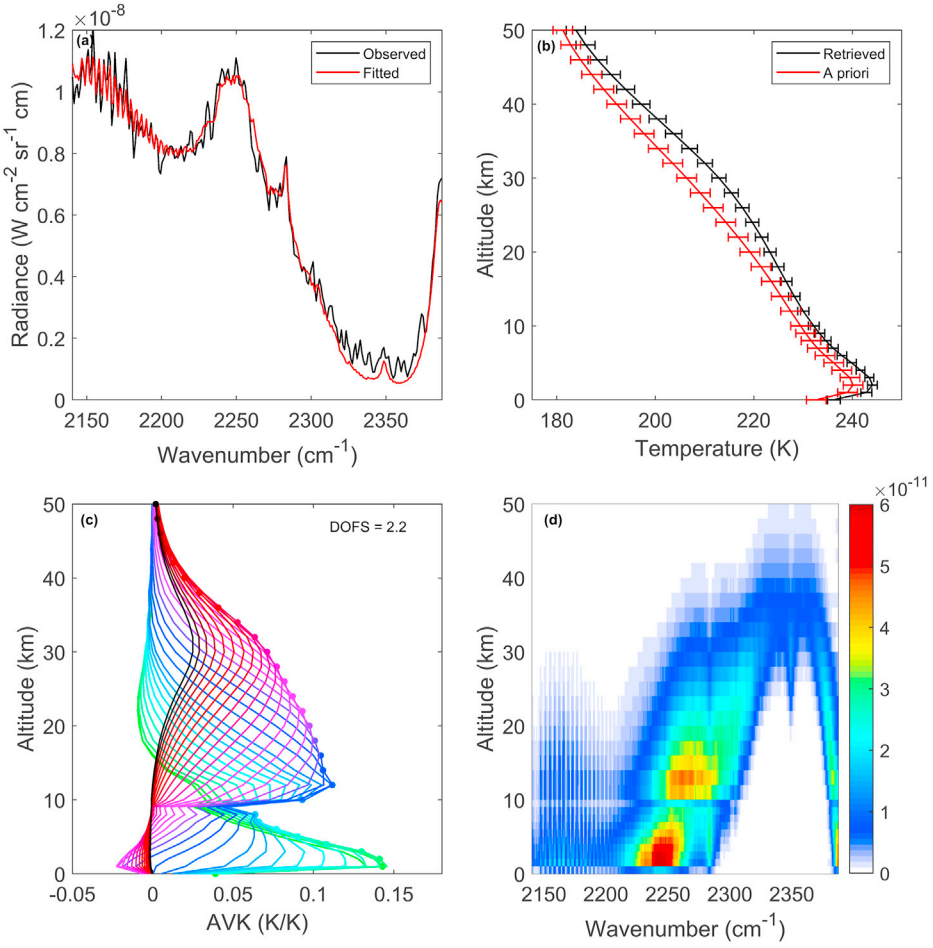

Fig. 12. Example of a temperature retrieval using the ν_3 band of CO_2 on an averaged spectrum built from only 7 single SWC PFS observations. (a) Resulting fit of the observed spectrum. (b) Retrieved and *a priori* temperature profiles with respectively the associated temperature retrieval error and *a priori* uncertainty. (c) Averaging kernel functions (K/K) from 0 to 50 km for the retrieval. The dots indicate to which level the AVK correspond. (d) Jacobians of temperature (color scale, W/(cm^2 sr cm^{-1}) per K) from 0 to 50 km.

and 4.5 K respectively for a surface pressure shift of +0.9 hPa and −0.9 hPa.

In conclusion, this work has shown that the retrieval performed on the ν_3 band of CO_2 provides a good knowledge of the temperature profile. The retrieved set of profiles obtained in this work is used for the retrieval of night-time CO abundance in a companion paper. In addition to be useful for the night-time CO retrieval, this work suggests that the CO_2 ν_3 band could be used along with the ν_2 band in future works to properly constrain and characterize the thermal inversions encountered near the surface for most night-time observations.

CRediT authorship contribution statement

Sophie Bauduin: Conceptualization, Methodology, Formal analysis, Investigation, Writing - review & editing, Visualization, Supervision. **Marco Giuranna:** Conceptualization, Resources, Writing - review & editing. **Paulina Wolkenberg:** Resources, Writing - review & editing. **Luca Nardi:** Writing - review & editing. **Frank Daerden:** Writing - review & editing. **Jimmy Bouche:** Writing - review & editing. **Catherine Wespes:** Writing - review & editing. **Gilles Lecomte:** Writing - review & editing. **Ann Carine Vandaele:** Writing - review & editing. **Pierre Coheur:** Conceptualization, Writing - review & editing.

Declaration of competing interest

The authors declare that they have no known competing financial interests or personal relationships that could have appeared to influence the work reported in this paper.

Acknowledgements

This work is partly funded by the F.R.S. FNRS CRAMIC project under grant number T.0171.16. The PFS experiment was built at the Institute for Space Astrophysics and Planetology (formerly the Institute for Interplanetary Space Physics) of the National Institute for Astrophysics, and is currently funded by the Italian Space Agency (agreement number 2018-2-HH.0) in the context of the science activities for NOMAD-ExoMars and for PFS-MEx. Sophie Bauduin is “Chargée de recherches” with F.R.S.-FNRS. The authors would like to thank the LMD for providing the access to the Mars Climate Database, which was used to build the *a priori* vertical profile CO and the associated covariance matrix.

References

Bandfield, J.L., 2002. Global mineral distributions on Mars. J. Geophys. Res.: Plan 107. https://doi.org/10.1029/2001JE001510.

Bauduin, S., Giuranna, M., Wolkenber, P., Nardi, L., Daerden, F., Bouche, J., Wespes, C., Lecomte, G., Vandaele, A.C., Coheur, P., 2020. Exploiting night-time averaged spectra from PFS/MEX shortwave channel. Part 2: near-surface CO retrievals. Planet. Space Sci. accepted.

Bertaux, J.L., Leblanc, F., Perrier, S., Quemerais, E., Korablev, O., Dimarellis, E., Reberac, A., Forget, F., Simon, P.C., Stern, S.A., Sandel, B., the Spicam team, 2005. Nightglow in the upper atmosphere of Mars and implications for atmospheric transport. Science 307, 566–569. https://doi.org/10.1126/science.1106957.

Billebaud, F., Brillet, J., Lellouch, E., Fouchet, T., Encrenaz, T., Cottini, V., Ignatiev, N., Formisano, V., Giuranna, M., Maturilli, A., Forget, F., 2009. Observations of CO in the atmosphere of Mars with PFS onboard Mars express. Planet. Space Sci. 57, 1446–1457. https://doi.org/10.1016/j.pss.2009.07.004.

Bouche, J., Bauduin, S., Giuranna, M., Robert, S., Aoki, S., Vandaele, A.C., Erwin, J.T., Daerden, F., Wolkenberg, P., Coheur, P.F., 2019. Retrieval and characterization of carbon monoxide (CO) vertical profiles in the Martian atmosphere from observations

of PFS/MEX. J. Quant. Spectrosc. Radiat. Transfer. https://doi.org/10.1016/j.jqsrt.2019.05.009.
Colaprete, A., Toon, O.B., 2002. Carbon dioxide snow storms during the polar night on Mars. J. Geophys. Res.: Plan 107. https://doi.org/10.1029/2001JE001758.
Cox, C., Saglam, A., Gérard, J.C., Bertaux, J.L., González-Galindo, F., Leblanc, F., Reberac, A., 2008. Distribution of the ultraviolet nitric oxide Martian night airglow: observations from Mars Express and comparisons with a one-dimensional model. J. Geophys. Res.: Plan 113. https://doi.org/10.1029/2007JE003037.
Forget, F., Hourdin, F., Fournier, R., Hourdin, C., Talagrand, O., Collins, M., Lewis, S.R., Read, P.L., Huot, J.P., 1999. Improved general circulation models of the Martian atmosphere from the surface to above 80 km. J. Geophys. Res. 104, 24155–24176. https://doi.org/10.1029/1999JE001025.
Forget, F., Montmessin, F., Bertaux, J.L., González-Galindo, F., Lebonnois, S., Quémerais, E., Reberac, A., Dimarellis, E., López-Valverde, M.A., 2009. Density and temperatures of the upper Martian atmosphere measured by stellar occultations with Mars Express SPICAM. J. Geophys. Res.: Plan 114. https://doi.org/10.1029/2008JE003086.
Formisano, V., Angrilli, F., Arnold, G., Atreya, S., Bianchini, G., Biondi, D., Blanco, A., Blecka, M.I., Coradini, A., Colangeli, L., Ekonomov, A., Esposito, F., Fonti, S., Giuranna, M., Grassi, D., Gnedykh, V., Grigoriev, A., Hansen, G., Hirsh, H., Khatuntsev, I., Kiselev, A., Ignatiev, N., Jurewicz, A., Lellouch, E., Lopez Moreno, J., Marten, A., Mattana, A., Maturilli, A., Mencarelli, E., Michalska, M., Moroz, V., Moshkin, B., Nespoli, F., Nikolsky, Y., Orfei, R., Orleanski, P., Orofino, V., Palomba, E., Patsaev, D., Piccioni, G., Rataj, M., Rodrigo, R., Rodriguez, J., Rossi, M., Saggin, B., Titov, D., Zasova, L., 2005. The planetary fourier spectrometer (PFS) onboard the European Mars express mission. Planet. Space Sci. 53, 963–974. https://doi.org/10.1016/j.pss.2004.12.006.
Gagné, M.E., Bertaux, J.L., González-Galindo, F., Melo, S.M.L., Montmessin, F., Strong, K., 2013. New nitric oxide (NO) nightglow measurements with SPICAM/MEx as a tracer of Mars upper atmosphere circulation and comparison with LMD-MGCM model prediction: evidence for asymmetric hemispheres. J. Geophys. Res.: Plan 118, 2172–2179. https://doi.org/10.1002/jgre.20165.
Giuranna, M., Formisano, V., Biondi, D., Ekonomov, A., Fonti, S., Grassi, D., Hirsch, H., Khatuntsev, I., Ignatiev, N., Malgoska, M., Mattana, A., Maturilli, A., Mencarelli, E., Nespoli, F., Orfei, R., Orleanski, P., Piccioni, G., Rataj, M., Saggin, B., Zasova, L., 2005a. Calibration of the planetary fourier spectrometer long wavelength channel. Planet. Space Sci. 53, 993–1007. https://doi.org/10.1016/j.pss.2005.02.007.
Giuranna, M., Formisano, V., Biondi, D., Ekonomov, A., Fonti, S., Grassi, D., Hirsch, H., Khatuntsev, I., Ignatiev, N., Michalska, M., Mattana, A., Maturilli, A., Moshkin, B.E., Mencarelli, E., Nespoli, F., Orfei, R., Orleanski, P., Piccioni, G., Rataj, M., Saggin, B., Zasova, L., 2005b. Calibration of the planetary fourier spectrometer short wavelength channel. Planet. Space Sci. 53, 975–991. https://doi.org/10.1016/j.pss.2004.12.007.
Giuranna, M., Viscardy, S., Daerden, F., Neary, L., Etiope, G., Oehler, D., Formisano, V., Aronica, A., Wolkenberg, P., Aoki, S., Cardesín-Moinelo, A., Marín-Yaseli de la Parra, J., Merritt, D., Amoroso, M., 2019a. Independent confirmation of a methane spike on Mars and a source region east of Gale Crater. Nat. Geosci. 12, 326–332. https://doi.org/10.1038/s41561-019-0331-9.
Giuranna, M., Wolkenberg, P., Grassi, D., Aronica, A., Aoki, S., Scaccabarozzi, D., Saggin, B., Formisano, V., 2019b. The current weather and climate of Mars: 12 years of atmospheric monitoring by the planetary fourier spectrometer on Mars express. Icarus. https://doi.org/10.1016/j.icarus.2019.113406.
Gordon, I.E., Rothman, L.S., Hill, C., Kochanov, R.V., Tan, Y., Bernath, P.F., Birk, M., Boudon, V., Campargue, A., Chance, K.V., Drouin, B.J., Flaud, J.M., Gamache, R.R., Hodges, J.T., Jacquemart, D., Perevalov, V.I., Perrin, A., Shine, K.P., Smith, M.A.H., Tennyson, J., Toon, G.C., Tran, H., Tyuterev, V.G., Barbe, A., Császár, A.G., Devi, V.M., Furtenbacher, T., Harrison, J.J., Hartmann, J.M., Jolly, A., Johnson, T.J., Karman, T., Kleiner, I., Kyuberis, A.A., Loos, J., Lyulin, O.M., Massie, S.T., Mikhailenko, S.N., Moazzen-Ahmadi, N., Müller, H.S.P., Naumenko, O.V., Nikitin, A.V., Polyansky, O.L., Rey, M., Rotger, M., Sharpe, S.W., Sung, K., Starikova, E., Tashkun, S.A., Auwera, J.V., Wagner, G., Wilzewski, J., Wcisło, P., Yu, S., Zak, E.J., 2017. The HITRAN2016 molecular spectroscopic database. J. Quant. Spectrosc. Radiat. Transf. 203, 3–69. https://doi.org/10.1016/j.jqsrt.2017.06.038.
Guerlet, S., Ignatiev, N., Fouchet, T., Forget, F., Millour, E., Young, R., Montabone, L., Grigoriev, A., Trokhimovskiy, A., Montmessin, F., Korablev, O., 2018. Thermal structure and aerosol content in the martian atmosphere from ACS-TIRVIM on board ExoMars/TGO. In: EPSC-DPS Joint Meeting 2018. EPSC2018–223–2.
Ivanov, A.B., Muhleman, D.O., 2001. Cloud reflection observations: results from the Mars orbiter laser altimeter. Icarus 154, 190–206. https://doi.org/10.1006/icar.2001.6686.
Lebonnois, S., Quémerais, E., Montmessin, F., Lefèvre, F., Perrier, S., Bertaux, J.L., Forget, F., 2006. Vertical distribution of ozone on Mars as measured by SPICAM/Mars Express using stellar occultations. J. Geophys. Res. 111, E09S05. https://doi.org/10.1029/2005JE002643.
Millour, E., Forget, F., Spiga, A., Vals, M., Zakharov, V., Montabone, L., Lefèvre, F., Montmessin, F., Chaufray, J.Y., Lòpez-Valverde, M.A., González-Galindo, F., Lewis, S.R., Read, P.L., Desjean, M.C., Cipriani, F., the Mcd development team, 2018. The Mars climate database (version 5.3). In: Scientific Workshop: from Mars Express to ExoMars (ESA-ESAC).
Montmessin, F., Bertaux, J.L., Quémerais, E., Korablev, O., Rannou, P., Forget, F., Perrier, S., Fussen, D., Lebonnois, S., Rébérac, A., Dimarellis, E., 2006. Subvisible CO_2 ice clouds detected in the mesosphere of Mars. Icarus 183, 403–410. https://doi.org/10.1016/j.icarus.2006.03.015.
Montmessin, F., Lefèvre, F., 2013. Transport-driven formation of a polar ozone layer on Mars. Nat. Geosci. 6, 930–933. https://doi.org/10.1038/NGEO1957.
Neumann, G.A., Smith, D.E., Zuber, M.T., 2003. Two Mars years of clouds detected by the Mars orbiter laser altimeter. J. Geophys. Res.: Plan 108. https://doi.org/10.1029/2002JE001849.
Pankine, A.A., Tamppari, L.K., 2015. Constraints on water vapor vertical distribution at the Phoenix landing site during summer from MGS TES day and night observations. Icarus 252, 107–120. https://doi.org/10.1016/j.icarus.2015.01.008.
Pettengill, G.H., Ford, P.G., 2000. Winter clouds over the north martian polar cap. Geophys. Res. Lett. 27, 609–612. https://doi.org/10.1029/1999GL010896.
Poulet, F., Quantin-Nataf, C., Ballans, H., Dassas, K., Audouard, J., Carter, J., Gondet, B., Lozac'h, L., Malapert, J.C., Marmo, C., Riu, L., Séjourné, A., 2018. PSUP: a planetary SUrface portal. Planet. Space Sci. 150, 2–8. https://doi.org/10.1016/j.pss.2017.01.016.
Quantin-Nataf, C., Lozac'h, L., Thollot, P., Loizeau, D., Bultel, B., Fernando, J., Allemand, P., Dubuffet, F., Poulet, F., Ody, A., Clenet, H., Leyrat, C., Harrisson, S., 2018. MarsSI: martian surface data processing information system. Planet. Space Sci. 150, 157–170. https://doi.org/10.1016/j.pss.2017.09.014.
Quémerais, E., Bertaux, J.L., Korablev, O., Dimarellis, E., Cot, C., Sandel, B.R., Fussen, D., 2006. Stellar occultations observed by SPICAM on Mars express. J. Geophys. Res.: Plan 111. https://doi.org/10.1029/2005JE002604.
Rodgers, C.D., 2000. Inverse Methods for Atmospheric Sounding: Theory and Practice. World scientific.
Schneider, N.M., Deighan, J.I., Jain, S.K., Stiepen, A., Stewart, A.I.F., Larson, D., Mitchell, D.L., Mazelle, C., Lee, C.O., Lillis, R.J., Evans, J.S., Brain, D., Stevens, M.H., McClintock, W.E., Chaffin, M.S., Crismani, M., Holsclaw, G.M., Lefevre, F., Lo, D.Y., Clarke, J.T., Montmessin, F., Jakosky, B.M., 2015. Discovery of diffuse aurora on Mars. Science 350. https://doi.org/10.1126/science.aad0313.
Smith, M.D., 2004. Interannual variability in TES atmospheric observations of Mars during 1999-2003. Icarus 167, 148–165. https://doi.org/10.1016/j.icarus.2003.09.010.
Stiepen, A., Gérard, J.C., Gagné, M.E., Montmessin, F., Bertaux, J.L., 2015. Ten years of Martian nitric oxide nightglow observations. Geophys. Res. Lett. 42, 720–725. https://doi.org/10.1002/2014GL062300.
Stiepen, A., Jain, S.K., Schneider, N.M., Deighan, J.I., González-Galindo, F., Gérard, J.C., Milby, Z., Stevens, M.H., Bougher, S., Evans, J.S., Stewart, A.I.F., Chaffin, M.S., Crismani, M., McClintock, W.E., Clarke, J.T., Holsclaw, G.M., Montmessin, F., Lefèvre, F., Forget, F., Lo, D.Y., Hubert, B., Jakosky, B.M., 2017. Nitric oxide nightglow and Martian mesospheric circulation from MAVEN/IUVS observations and LMD-MGCM predictions. J. Geophys. Res.: Space Physics 122, 5782–5797. https://doi.org/10.1002/2016JA023523.
Wolkenberg, P., Giuranna, M., Grassi, D., Aronica, A., Aoki, S., Scaccabarozzi, D., Saggin, B., 2018. Characterization of dust activity on Mars from MY27 to MY32 by PFS-MEX observations. Icarus 310, 32–47. https://doi.org/10.1016/j.icarus.2017.10.045.